Ablation Study to Derive a Computationally Efficient Deep Learning-Based Super-Resolution Approach

Asfa Jamil* and Alessandro Artusi†
* CYENS- Center of Excellence E-mail: asfajamil164@outlook.com Tel/Fax: +353-852006837
† CYENS- Center of Excellence E-mail: a.artusi@cyens.org.cy

***Abstract*—Recent research on single-image super-resolution (SR) shows that deep learning-based methods outperform state-of-the-art techniques but at the cost of increased memory consumption and computational complexity. This results in longer training and inference times and higher GPU memory requirements compared to traditional approaches. Network architecture modifications can impact performance, complexity, and memory needs. This paper explores enhancing SR performance using a simple yet efficient deep-learning SR model, focusing on local and global connections in residual networks, channel attention mechanisms, and up-sampling techniques. Our efficient, lightweight, locally dense residual SR architecture achieves performance comparable to state-of-the-art models, reducing spatial complexity by up to 1/6 and inference time by half compared to the baseline.**

I. Introduction and Related Work

Single Image Super-Resolution (SR) enhances the resolution of low-resolution images to generate high-resolution counterparts [2]. This process focuses on restoring high-frequency information lost during image acquisition or compression [3], significantly improving visual quality. SR has diverse applications in computer vision, including enhancing medical images, improving surveillance footage, and analyzing satellite imagery [4],

Deep learning-based SR methods have emerged as superior, leveraging neural networks to learn complex mappings from low-resolution to high-resolution images, producing sharper outputs. Convolutional Neural Network (CNN)-based architectures, such as SRCNN [5] and FSRCNN [6], stack convolutional layers to map low to high-resolution images. ResNet and Recurrent Neural Network (RNN)-based architectures, like DRCN [7] and DRRN [8], use recursion and residual learning for better efficiency. EDSR [9] simplifies SRResNet, and CARN [10] offers a lightweight network for fast SR. Dense-connection-based architectures, such as SRDenseNet [11], improve learning by propagating information from early to later layers. Generative Adversarial Networks (GANs), like Relativistic GAN [12] and ESRGAN [13], produce realistic textures by using a generator and discriminator network. Channel attention-based architectures, like RCAN [14], focus on informative features using attention mechanisms.

Despite their effectiveness, deep learning methods face challenges due to their complexity, leading to high memory usage and computational inefficiency during inference. These multi-layered neural networks demand substantial computational resources during training and execution, posing scalability constraints. Studies show that modifying neural network architecture, loss function, and learning approach can affect performance quality, network complexity, and memory requirements [12]. Previous research [15] demonstrated that minimizing the complexity of state-of-the-art deep-learning SR methods, like DRLN [1], can achieve cost-effective solutions without sacrificing performance. This approach reduced spatial complexity by up to 1/6 and inference time by half compared to the baseline model.

Inspired by this, we propose a novel deep-learning SR model that minimizes spatial complexity and memory usage while enhancing computational efficiency. We tested the model on various datasets and up-sampling scales (e.g., 2×, 3×, 4×, 8×) and compared it with top-performing SR methods. Its efficiency makes it suitable for integration into scenarios such as encoding/decoding standards, editing tools, satellite imaging, and embedded systems.

The main contributions of our work are: noitemsep

1) An ablation study to identify optimal combinations for a DNN-based SR method.
2) Investigating strategies like local and global dense residual connections, pre/post and iterative up-sampling methods, and various pooling strategies in Laplacian attention modules to enhance SR performance.
3) Evaluating how these strategies impact the network's structural complexity, spatial complexity, and computational cost.
4) Developing an SR model that achieves comparable results to state-of-the-art models while reducing spatial complexity by one-sixth and halving training/inference time.

This paper is structured as follows: Section II presents our proposed model. Section III outlines experimental procedures and results. Section IV concludes the paper.

II. Proposed Architecture

The overall deep-learning structure of the proposed model is depicted in Figure 2. The architecture incorporates local dense cascading residual connections, enabling the network to effectively capture complex patterns. An attention mechanism is also employed that selectively emphasizes important regions of the input image, enhancing feature relevance. The network employs an iterative up-sampling technique to incrementally improve image resolution and a sub-pixel up-sampling technique to rearrange pixel values and enhance resolution. Finally, the network is trained using an L1 loss function, which

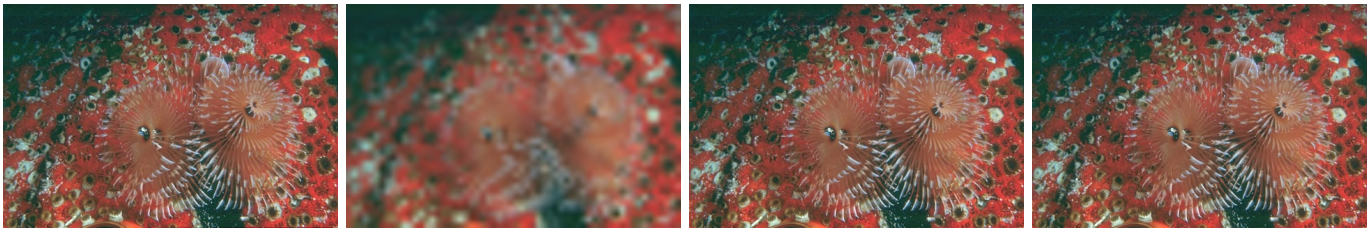

Fig. 1. Super-resolution is a process to increase the spatial resolution of an input image, with the intent of improving its overall spatial information. Here we show results comparing the ground truth high resolution image (left), compared to the up-sampled images using (left-center) bi-cubic interpolation, (right-center) a state-of-the-art deep-learning based approach [1] and (right) the proposed solution.

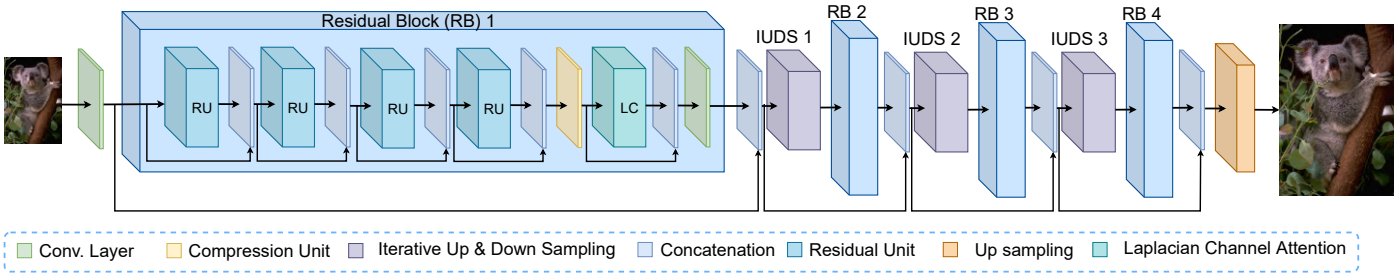

Fig. 2. The proposed SR architecture includes key components: the Residual Block (RB) and Iterative Up Down-Sampling (IUDS). The RB contains the Residual Unit (RU) and Laplacian Channel Attention (LC), which uses a Laplacian pyramid mechanism for multi-scale behavior. The IUDS incorporates up-sampling and down-sampling mechanisms.

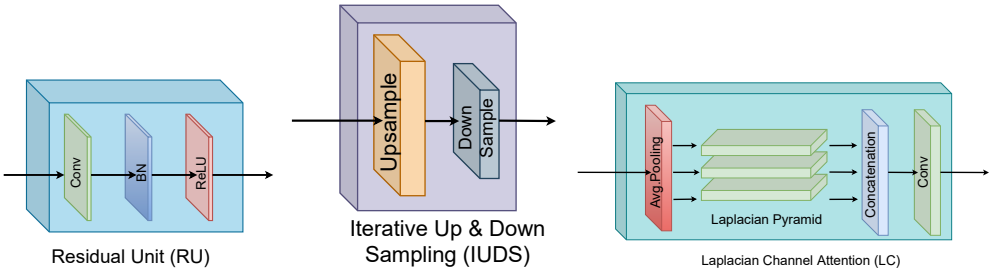

Fig. 3. Major components of the Residual Block: (left) Iterative Up-Sampling; (center) Residual Unit; (right) Laplacian Channel Attention.

measures the absolute differences between the predicted and ground-truth images. Overall, our proposed architecture is designed to produce high-quality output images while minimizing the network's complexity and memory requirements.

Cascading Residual over Residual Block Our model is composed of four cascading residual over residual blocks, which we will continue to refer to as Residual Blocks (RB) for simplicity. These blocks are designed to gradually learn complex features in the input image, allowing the model to generate high-quality super-resolved images. Each RB in our model consists of 4 Residual Units (RU), each followed by a concatenation layer. This design allows the model to learn residual functions more effectively, by incorporating information from earlier into later ones.

Residual Unit Each Residual Block (RB) is built from a lightweight Residual Unit (RU), consisting of one convolutional layer, one ReLU layer, and one batch normalization layer (Figure 3, left). This streamlined design enhances efficiency and ease of training. As shown in Table I for the 2X up-sampling factor, our model achieves comparable PSNR scores while halving memory usage and being 25% more computationally efficient. Figure 4(a) shows the visual qualitative result of the lightweight RU compared to the traditional one, with clearer details and less noise on the zebra skin.

Laplacain Channel (LC) attention module Following the last Residual Unit (RU), we include a compression layer, a Laplacian attention unit, a concatenation layer, and a convolutional layer.

The Laplacian Channel (LC) attention module enhances significant image features using a Laplacian pyramid approach, which weights important sub-band features. It employs a global descriptor for image statistics and a gating mechanism for channel dependencies (Figure 3, right).

The global descriptor processes the output from the compression unit, which has c feature maps of size $h \times w$. The Laplacian pyramid weights are computed using convolutional layers with specified kernel dilation. The pyramid output is convolved, down-sampled, up-sampled, and passed through a sigmoid activation function, adaptively re-scaling the output.

In our findings, tt has demonstrated effectiveness on the

MANGA109 dataset, providing crisper and better-represented details, as shown in Figure 4(b). The upper zoomed area in Figure 4(b) shows the improved detail using the LC module compared to the bottom zoomed area without it.

Local vs Global dense connections Our architecture emphasizes localized dense connections over global ones, featuring more dense local connections between residual units than global connections between residual blocks. Our findings highlight that this approach preserves intricate details, optimizes parameter efficiency, enhances gradient flow, and maintains feature hierarchy with reduced computational overhead. This underscores the importance of focusing on local dense mechanisms for tasks that require high-resolution detail conservation. Figure 4(c) shows the results for the 2x up-sampling factor case. When long residual connections are used (top zoomed area), crisper details are observed compared to the bottom area in the same figure, where long residual connections are not used.

Iterative Up/Down-Sampling Framework

We propose iterative up-sampling and down-sampling modules (Figure 3, center) to enhance network performance. These modules adjust the resolution of feature maps during processing.

Up-Sampling Module: The up-sampling module uses a sub-pixel layer to rearrange pixels and increase feature map resolution:

$$F_{up} = P \times (R \times F_{low})$$

where F_{up} is the up-sampled feature map, P is the pixel shuffle operation, R is the up-scaling factor, and F_{low} is the input low-resolution feature map. This is followed by batch normalization and ReLU activation.

Down-Sampling Module: The down-sampling module uses a MaxPool2d layer to reduce feature map resolution:

$$F_{down} = \max_{i,j \in W} (F_{up}(i,j))$$

where F_{down} is the down-sampled feature map, F_{up} is the input high-resolution feature map, W is the pooling window, and i and j are indices in the pooling window.

Table I and Figure 4(d) show that the IUDS module improves image details without increasing model complexity, memory usage, or computation time.

TABLE I
PERFORMANCE COMPARISONS FOR 2X UP-SAMPLING FACTOR ON THE B100 DATASET [16].

Metrics	TRU	LRU	No IUS	With IUS
GPU memory(MB)	4414	2555	2417	2555
Run-time (s)	0.27	0.187	0.18	0.187
PSNR	32.097	32.069	32.055	32.069

TRU = Traditional RU, LRU = Lightweight RU, IUS = Iterative up-sampling

III. EXPERIMENTAL RESULTS

We have tested the proposed model on a variety of standard benchmark data sets, i.e., URBAN100, B100, SET14, and SET5 . To demonstrate its robustness we have applied the proposed model to different types of up-sampling factors from $2\times$ to $8\times$. We have evaluated the proposed models on the following characteristics: image quality (PSNR and SSIM scores), spatial complexity, and inference time. Spatial complexity is measured as occupied on-board GPU memory, and the methodology to calculate GPU memory occupation is the one used in [25].

Training Settings: The experiments have been performed on a computer with an Intel Core i7-8700k processor running at 3.70 GHz, using 32 GB RAM, and NVIDIA GeForce RTX 2080Ti GPU. The model has been trained using the DIV2k[26] data set. In our training settings, we maintain a batch size of 4 and start with an initial learning rate of 10^{-4}. This rate is halved every 2^4 iterations. We employ the ADAM optimizer, setting the initial parameters to $\beta_1 = 0.9$, $\beta_2 = 0.999$, and $\epsilon = 10^{-8}$.

Overall Comparison for $2\times$, $3\times$, $4\times$, and $8\times$ Up-Sampling: This section compares the proposed model with state-of-the-art SR methods in terms of PSNR, SSIM, inference time, and GPU memory consumption for $2\times$, $3\times$, $4\times$, and $8\times$ up-sampling factors. First, the quantitative analysis of the proposed method is shown in Section III-1. Then, the spatial complexity and efficiency is analyzed in Section III-2, and finally, Section III-3 provides the visual quality comparison at different up-scaling factors, all compared to the state-of-the-art methods.

1) Quantitative Analysis of Proposed Model: Tables III to VI compare the PSNR and SSIM scores of our model against existing high-performance methods.

For 2x upsampling, our model performs competitively across all datasets, achieving PSNR scores of 33.50 dB on SET14 and 31.96 dB on URBAN100, with SSIM scores of 0.92 for both. These results are comparable to EDSR and RCAN. At 3x upsampling, our model records PSNR values of 30.28 dB on SET14 and 29.04 dB on BSD100, with SSIM scores of 0.84 and 0.80, respectively, closely matching RDN and RCAN. For 4x upsampling, our model achieves PSNR scores of 28.72 dB on SET14 and 26.34 dB on URBAN100, with SSIM scores of 0.78 and 0.80, slightly trailing DRLN and RCAN. At 8x upsampling, our model reaches PSNR scores of 24.84 dB on SET14 and 22.97 dB on URBAN100, with SSIM scores of 0.62 and 0.61, slightly below DRLN and RCAN. These comparisons show that our model consistently delivers high-quality images across various up-sampling sizes, demonstrating its effectiveness and adaptability.

2) Spatial Complexity and Efficiency Analysis: The spatial complexity of a deep-learning model, measured by on-board GPU memory consumption [25], is crucial for practical applications. Figures 5 and 7 show these results.

Figure 5 highlights the spatial complexity of our proposed model compared to SOTA methods across resolutions of 320x240, 720x480, and 1920x1080. Our model uses significantly less memory, about $1/13^{th}$ and $1/5^{th}$ of the GPU memory compared to EDSR and RCAN at 320x240, maintaining efficiency even at 1920x1080.

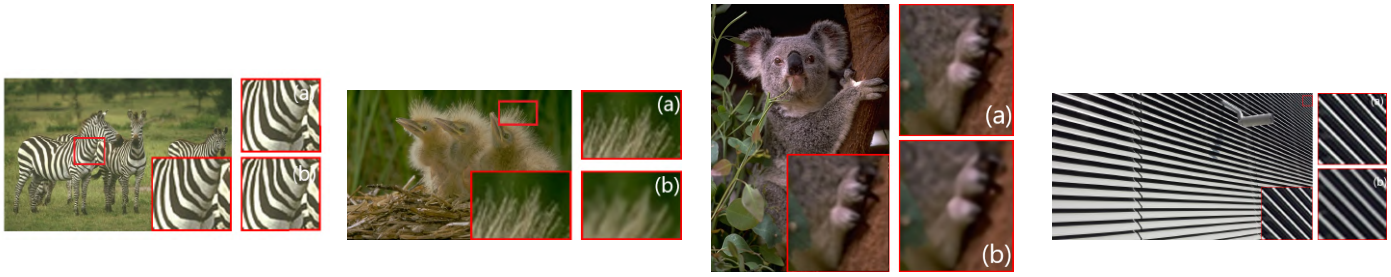

Fig. 4. Qualitative comparisons on 3x up-sampling factor: (a) Traditional vs. lightweight RU, (b) Incorporating Laplacian attention unit, (c) SR technique with and without global residual connections, (d) Proposed model with and without IUDS unit.

TABLE II

QUANTITATIVE EVALUATION OF COMPETING METHODS ON 2X AND 3X UP-SAMPLING FACTORS. WE REPORT THE PERFORMANCE OF STATE-OF-THE-ART ALGORITHMS AND THE PROPOSED MODEL ON WIDELY USED PUBLICLY AVAILABLE DATASETS, IN TERMS OF PSNR (IN DB) AND SSIM SCORES.

TABLE III

2X UP-SAMPLING FACTOR

Method	SET5		SET14		BSD100		URBAN100	
Bicubic	33.66	0.9299	30.24	0.8688	29.56	0.8431	26.88	0.8403
SRCNN [17]	36.66	0.9542	32.45	0.9067	31.36	0.8879	29.50	0.8946
FSRCNN [18]	37.05	0.9560	32.66	0.9090	31.53	0.8920	29.88	0.9020
VDSR [19]	37.53	0.9590	33.05	0.9130	31.90	0.8960	30.77	0.9140
LapsRN [20]	37.52	0.9591	33.08	0.9130	31.08	0.8950	30.41	0.9101
EDSR [21]	38.11	0.9602	33.92	0.9195	32.32	0.9013	32.93	0.9351
RDN [22]	38.24	0.9614	34.01	0.9212	32.34	0.9017	32.89	0.9353
RCAN [23]	38.27	0.9614	34.12	0.9216	32.41	0.9027	33.34	0.9384
CARN[24]	37.76	0.9590	33.52	0.9166	32.09	0.8978	31.92	0.9256
DRLN[1]	38.27	0.9616	34.28	0.9231	32.44	0.9028	33.37	0.9390
Our Model	37.95	0.9611	33.50	0.9212	32.11	0.9015	32.96	0.9266

TABLE IV

3X UP-SAMPLING FACTOR

Method	SET5		SET14		BSD100		URBAN100	
Bicubic	30.39	0.8682	27.55	0.7742	27.21	0.7385	24.46	0.7349
SRCNN[17]	32.75	0.9090	29.30	0.8215	28.41	0.7863	26.24	0.7989
FSRCNN[18]	33.18	0.9140	29.37	0.8240	28.53	0.7910	26.43	0.8080
VDSR[19]	33.67	0.9210	29.78	0.8320	28.83	0.7990	27.14	0.8290
LapsRN[20]	33.82	0.9227	29.87	0.8320	28.82	0.7980	27.07	0.8280
EDSR [21]	34.65	0.9280	30.52	0.8462	29.25	0.8093	28.80	0.8653
RDN[22]	34.71	0.9296	30.57	0.8468	29.26	0.8093	28.80	0.8653
RCAN [23]	34.74	0.9299	30.65	0.8482	29.32	0.8111	29.09	0.8702
CARN[24]	34.29	0.9255	30.29	0.8407	29.06	0.8034	28.06	0.8493
DRLN [1]	34.78	0.9303	30.73	0.8488	29.36	0.8117	29.21	0.8722
Our Model	34.30	0.9300	30.28	0.8460	29.04	0.8112	28.10	0.8689

TABLE V

4X UP-SAMPLING FACTOR

Method	SET5		SET14		BSD100		URBAN100	
Bicubic	28.42	0.8104	26.00	0.7027	25.96	0.6675	23.14	0.6577
SRCNN [17]	30.48	0.8628	27.50	0.7513	26.90	0.7101	24.52	0.7221
FSRCNN [18]	30.72	0.8660	27.61	0.7550	26.98	0.7150	24.62	0.7280
VDSR [19]	31.35	0.8830	28.02	0.7680	27.29	0.7276	25.18	0.7540
LapSRN [20]	31.54	0.8850	28.19	0.7720	27.32	0.7270	25.21	0.7560
EDSR [21]	32.46	0.8968	28.80	0.7876	27.71	0.7420	26.64	0.8033
RDN [22]	32.47	0.8990	28.81	0.7871	27.72	0.7419	26.61	0.8028
RCAN [23]	32.63	0.9002	28.87	0.7889	27.77	0.7436	26.82	0.8087
CARN [24]	32.13	0.8937	28.60	0.7806	27.58	0.7349	26.07	0.7837
DRLN [1]	32.63	0.9002	28.94	0.7900	27.83	0.7444	26.98	0.8119
Our Model	32.19	0.8987	28.72	0.7860	27.57	0.7435	26.34	0.8067

TABLE VI

8X UP-SAMPLING FACTOR

Method	SET5		SET14		BSD100		URBAN100	
Bicubic	24.40	0.6580	23.10	0.5660	23.67	0.5480	20.70	0.5160
SRCNN [17]	25.33	0.6900	23.76	0.5910	24.13	0.5660	21.29	0.5440
FSRCNN [18]	20.13	0.5520	19.75	0.4820	24.21	0.5680	21.32	0.5380
VDSR **vdsr**	25.93	0.7240	24.26	0.6140	24.49	0.5830	21.70	0.5710
LapSRN [20]	26.15	0.7380	24.35	0.6200	24.54	0.5860	21.81	0.5810
EDSR [21]	26.96	0.7762	24.91	0.6420	24.81	0.5985	22.51	0.6221
RCAN [23]	27.31	0.7878	25.23	0.6511	24.98	0.6058	23.00	0.6452
DRLN [1]	27.36	0.7882	25.34	0.6531	25.01	0.6057	23.06	0.6471
Our Model	26.94	0.7700	24.84	0.6290	24.71	0.5990	22.97	0.6151

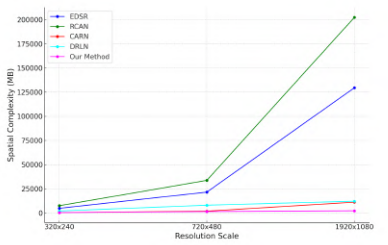

Fig. 5. Comparison of spatial complexity of the proposed model and state-of-the-art at resolutions 320x240, 720x480, and 1920x1080.

Figures 7 provide a detailed comparison of spatial complexity. At 4x upscaling on the B100 dataset (Figure 7), our model operates with approximately $1/5^{th}$ the spatial complexity of EDSR and RCAN. For 8x upscaling on the Urban100 dataset, our model requires just $1/6^{th}$ the spatial complexity of models like RCAN, while delivering impressive PSNR and SSIM scores.

Overall, our model consistently delivers high-quality super-resolution with significantly reduced spatial complexity compared to SOTA models such as RCAN, EDSR, and DRLN.

We also compared our model's computational efficiency in terms of inference time. Figure 8 shows the inference time per image and PSNR score on the B100 dataset [16]. The proposed model reduces inference time by approximately 50% across 2x, 3x, 4x, and 8x resolutions.

3) Comparing Visual Quality at Different Up-sampling Levels: Figure 6 visually compares our model's performance at 2x, 3x, 4x, and 8x upscaling against benchmarks: (a) ground truth, (b) bicubic interpolation, (c) SRCNN, (d) CARN, (e) EDSR, (f) RCAN, and (g) DRLN, with our model shown in (h). These comparisons highlight our model's ability to enhance image clarity, outperforming methods (c) and (d), and competing well with methods (e), (f), and (g). At 8x upscaling, our model matches ground truth and DRLN quality while improving computational efficiency by 50% and reducing spatial complexity by nearly $1/5^{th}$.

IV. CONCLUSIONS

This paper analyzes the architecture of state-of-the-art deep learning SISR models, focusing on performance, memory needs, and computational costs. We propose a lightweight

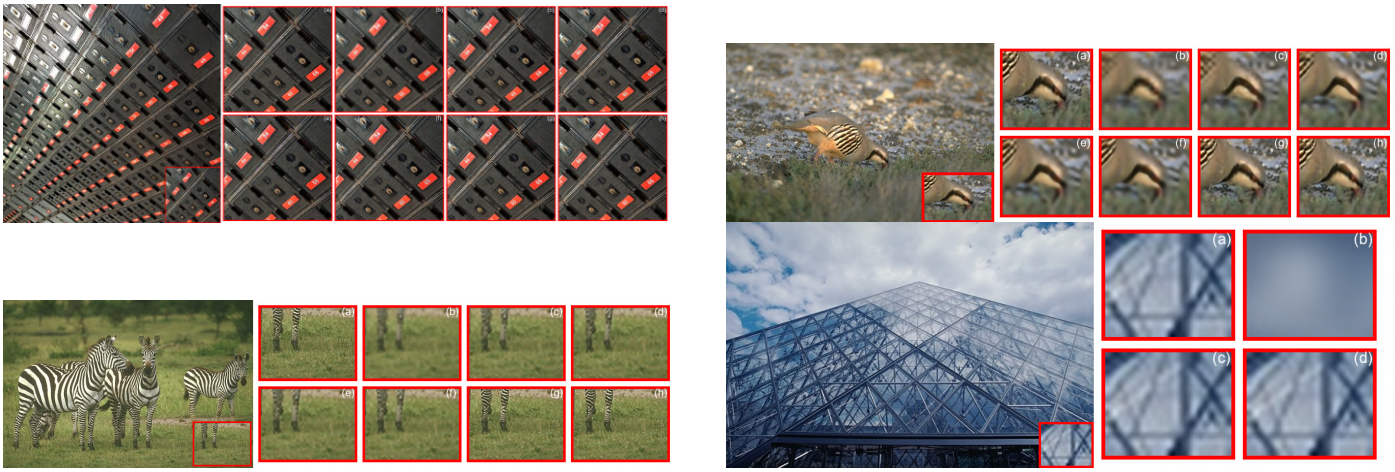

Fig. 6. Qualitative comparison of our models with other works on super-resolution for different up-sampling factors: (a) 2x, (b) 3x, (c) 4x, and (d) 8x. Each subfigure demonstrates the performance of our proposed model relative to existing methods, featuring (a) ground truth, (b) bicubic interpolation, and results from various methods including SRCNN, CARN, EDSR, RCAN, and DRLN, with our proposed model shown last.

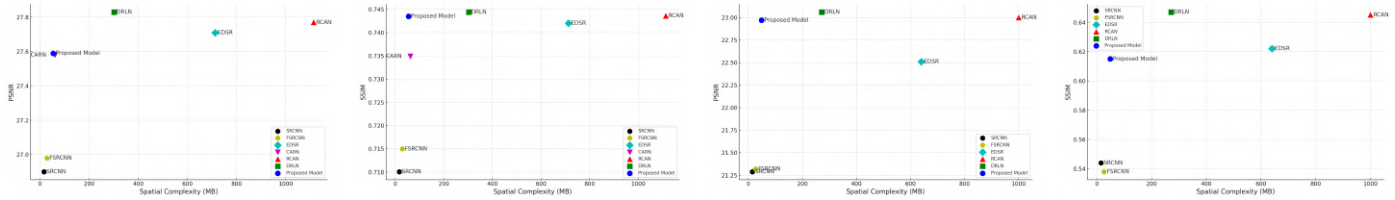

Fig. 7. (a) PSNR vs. Spatial Complexity at 4x resolution for B100 dataset. (b) SSIM vs. Spatial Complexity at 4x resolution for B100 dataset. (c) PSNR vs. Spatial Complexity at 8x resolution for Urban100 dataset. (d) SSIM vs. Spatial Complexity at 8x resolution for Urban100 dataset.

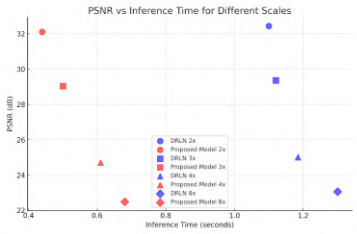

Fig. 8. Comparison of PSNR vs. inference time between state-of-the-art DRLN and proposed model at 2x, 3x, 4x, and 8x resolution for B100 dataset.

SISR model that is spatially efficient and computationally effective. Our model reduces inference time by approximately 50% compared to DRLN and supports upscaling factors from 2x to 8x, as demonstrated on benchmark datasets. It consumes only 1/6th of the GPU memory of state-of-the-art models while maintaining competitive PSNR and SSIM scores. Our model achieves superior visual quality compared to other lightweight alternatives and matches the performance of more computationally intensive models like EDSR, RCAN, and DRLN.

REFERENCES

[1] S. Anwar and N. Barnes, "Densely residual laplacian super-resolution," *IEEE Transactions on Pattern Analysis and Machine Intelligence*, 2020.

[2] C. Zhong and Y. Zhou, "Progressive low/high-resolution space attention fusion network for single image super-resolution," *Journal of Physics: Conference Series*, vol. 1828, no. 1, pp. 12–21, Feb. 2021. DOI: 10.1088/1742-6596/1828/1/012021. [Online]. Available: http://dx.doi.org/10.1088/1742-6596/1828/1/012021.

[3] H. Liu, Z. Fu, J. Han, L. Shao, S. Hou, and Y. Chu, "Single image super-resolution using multi-scale deep encoder–decoder with phase congruency edge map guidance," *Information Sciences*, vol. 473, pp. 44–58, 2019, ISSN: 0020-0255. [Online]. Available: https://doi.org/10.1016/j.ins.2018.09.018.

[4] Y. Li, B. Sixou, and F. Peyrin, "A review of the deep learning methods for medical images super resolution problems," *Irbm*, vol. 42, no. 2, pp. 120–133, 2021.

[5] C. Dong, C. C. Loy, K. He, and X. Tang, "Image super-resolution using deep convolutional networks," *IEEE transactions on pattern analysis and machine intelligence*, vol. 38, no. 2, pp. 295–307, 2015.

[6] C. Dong, C. C. Loy, and X. Tang, "Accelerating the super-resolution convolutional neural network," in *Eu-*

ropean conference on computer vision, Springer, 2016, pp. 391–407.

[7] J. Kim, J. K. Lee, and K. M. Lee, "Deeply-recursive convolutional network for image super-resolution," in *Proceedings of the IEEE conference on computer vision and pattern recognition*, 2016, pp. 1637–1645.

[8] Y. Tai, J. Yang, and X. Liu, "Image super-resolution via deep recursive residual network," in *Proceedings of the IEEE conference on computer vision and pattern recognition*, 2017, pp. 3147–3155.

[9] B. Lim, S. Son, H. Kim, S. Nah, and K. Mu Lee, "Enhanced deep residual networks for single image super-resolution," in *Proceedings of the IEEE conference on computer vision and pattern recognition workshops*, 2017, pp. 136–144.

[10] N. Ahn, B. Kang, and K.-A. Sohn, "Fast, accurate, and lightweight super-resolution with cascading residual network," in *Proceedings of the European Conference on Computer Vision (ECCV)*, 2018, pp. 252–268.

[11] T. Tong, G. Li, X. Liu, and Q. Gao, "Image super-resolution using dense skip connections," in *Proceedings of the IEEE international conference on computer vision*, 2017, pp. 4799–4807.

[12] S. Zhang, D. Cheng, D. Jiang, and Q. Kou, "Least squares relativistic generative adversarial network for perceptual super-resolution imaging," *IEEE Access*, vol. 8, pp. 185 198–185 208, 2020.

[13] X. Wang, K. Yu, S. Wu, *et al.*, "Esrgan: Enhanced super-resolution generative adversarial networks," in *Proceedings of the European conference on computer vision (ECCV) workshops*, 2018, pp. 0–0.

[14] Y. Zhang, K. Li, K. Li, L. Wang, B. Zhong, and Y. Fu, "Image super-resolution using very deep residual channel attention networks," in *Proceedings of the European conference on computer vision (ECCV)*, 2018, pp. 286–301.

[15] A. Jamil and A. Artusi, "Computational efficient deep learning-based super resolution approach," in *Real-time Processing of Image, Depth and Video Information 2023*, M. F. Carlsohn, Ed., International Society for Optics and Photonics, vol. 12571, SPIE, 2023, 125710E. DOI: 10.1117/12.2665645. [Online]. Available: https://doi.org/10.1117/12.2665645.

[16] D. Martin, C. Fowlkes, D. Tal, and J. Malik, "A database of human segmented natural images and its application to evaluating segmentation algorithms and measuring ecological statistics," in *Proceedings Eighth IEEE International Conference on Computer Vision. ICCV 2001*, IEEE, vol. 2, 2001, pp. 416–423.

[17] C. M. Ward, J. Harguess, B. Crabb, and S. Parameswaran, "Image quality assessment for determining efficacy and limitations of super-resolution convolutional neural network (srcnn)," in *Applications of Digital Image Processing XL*, SPIE, vol. 10396, 2017, pp. 19–30.

[18] L. S. Passarella, S. Mahajan, A. Pal, and M. R. Norman, "Reconstructing high resolution esm data through a novel fast super resolution convolutional neural network (fsrcnn)," *Geophysical Research Letters*, vol. 49, no. 4, e2021GL097571, 2022.

[19] S. Hitawala, Y. Li, X. Wang, and D. Yang, "Image super-resolution using vdsr-resnext and srcgan," *arXiv preprint arXiv:1810.05731*, 2018.

[20] W.-S. Lai, J.-B. Huang, N. Ahuja, and M.-H. Yang, "Deep laplacian pyramid networks for fast and accurate super-resolution," in *Proceedings of the IEEE conference on computer vision and pattern recognition*, 2017, pp. 624–632.

[21] B. M. Kuriakose *et al.*, "Edsr: Empowering super-resolution algorithms with high-quality div2k images," *Intelligent Decision Technologies*, no. Preprint, pp. 1–15,

[22] G. Chen, L. Zhang, M. Sun, Y. Gao, P. N. Michelini, and Y. Wu, "Single-image hdr reconstruction with task-specific network based on channel adaptive rdn," in *Proceedings of the IEEE/CVF Conference on Computer Vision and Pattern Recognition*, 2021, pp. 398–403.

[23] Z. Lin, P. Garg, A. Banerjee, *et al.*, "Revisiting rcan: Improved training for image super-resolution," *arXiv preprint arXiv:2201.11279*, 2022.

[24] Y. Li, E. Agustsson, S. Gu, R. Timofte, and L. Van Gool, "Carn: Convolutional anchored regression network for fast and accurate single image super-resolution," in *Proceedings of the European Conference on Computer Vision (ECCV) Workshops*, 2018, pp. 0–0.

[25] A. Jamil and A. Artusi, "Computational efficient deep learning-based super resolution approach," in *Real-time Processing of Image, Depth and Video Information 2023*, SPIE, vol. 12571, 2023, pp. 114–121.

[26] R. Timofte, E. Agustsson, L. Van Gool, M.-H. Yang, and L. Zhang, "Ntire 2017 challenge on single image super-resolution: Methods and results," in *Proceedings of the IEEE conference on computer vision and pattern recognition workshops*, 2017, pp. 114–125.